



I S A V

**Journal of Theoretical and Applied
Vibration and Acoustics**

journal homepage: <http://tava.isav.ir>



Evaluation of cantilever plates in the spinning situation: time histories and modal characteristics

Hamidreza Rostami^a, Firooz Bakhtiari-Nejad^{b*}, Amirhossein Modarres-Aval^c, Earl H Dowell^d

^aPhD, Department of Ocean Engineering, Amirkabir University of Technology, Tehran, Iran

^bProfessor, Department of Mechanical Engineering, University of Maryland at Baltimore County, USA & Department of Mechanical Engineering, Amirkabir University of Technology, Tehran, Iran

^cPhD Student, Department of Mechanical Engineering, Amirkabir University of Technology, Tehran, Iran

^d Professor, Department of Mechanical Engineering, Duke University Durham, North Carolina, USA

ARTICLE INFO

Article history:

Received 20 January 2020

Received in revised form
5 March 2020

Accepted 26 April 2020

Available online 30 April 2020

Keywords:

Rotating blade,

Cantilever plates,

Orthotropic plates,

Modal characteristics,

System response.

ABSTRACT

A study on the dynamics of cantilever orthotropic plates under spinning conditions is presented in this article. The governing equations of motions are containing the centrifugal and Coriolis effects. Two approximation methods, the extended Galerkin method, and extended Kantorovich method, are utilized for the investigation of the mathematical model. The verification of the obtained results is conducted by comparing two methods that show good agreement. This investigation is concentrated on the time histories and the natural frequencies of the system. First, using time responses, the effects of different types and numbers of admissible functions used in the approximate solution are discussed. Next, the results are obtained to explore the impact of dimensionless parameters like material, hub radius ratio, stagger angle, etc. on the modal characteristics of the spinning structures. The results of the simulations exhibit the importance of the proper choice of both type and number for trial functions. Furthermore, the selection of orthogonal functions can be vital to guarantee the convergence speed of an approximate solution. Further discussion on the modal characteristic reveals that in different stiffness ratios of the plate, the centrifugal stiffening rate caused by spinning motion is affected by rotational speed. Moreover, this stiffening rate is depended on setting angle and hub radius ratio. Finally, the last part of the paper is devoted to the forced response analysis of the rotating plate.

© 2020 Iranian Society of Acoustics and Vibration, All rights reserved.

* Corresponding author:

E-mail address: bakhtiari@aut.ac.ir (F. Bakhtiari-Nejad)

<http://dx.doi.org/10.22064/tava.2020.121868.1155>

1.Introduction

Rotating blades, which have importance in many practical applications such as propellers and turbine blades, have been modeled as a rotating plate. Evaluation of these complicated systems can be helpful to detect and characterize the minor failures which can lead to catastrophic events.

Previous investigations have focused on isotropic plates. Dokainish and Rawtani [1] utilized a finite element technique to determine the natural frequencies of an isotropic plate. Wang *et al.* [2] employed the Galerkin method to calculate the natural frequency of a rotating isotropic plate. Rao and Gupta [3] presented an analysis of the free vibration of a rotating small aspect ratio blade. Refs.[4, 5] investigated the effects of different parameters on the modal characteristics of vibrations of a rotating isotropic plate. A dynamic modeling method, which employs the Kane and Rayleigh–Ritz methods, was introduced by Yoo and Kim, for the vibration analysis of rotating plates[6]. Yoo *et al.* [7] extended the approach to the vibration analysis of rotating composite plates. Sinha and Turner [5] derived the equation of motion of rotating plates, where the effect of warping of the cross-section is included. A forced response analysis was performed by Sun *et al.* [4] to determine the effect of damping on the dynamic response of the rotating plate. During recent years, the dynamics of rotating orthotropic plates have received considerable attention. Based on the assumed modes method and Lagrange’s equations, the equations of a functionally graded plate are developed by Li and Zhang [8]. Sinha and Zylka [9] applied the Rayleigh-Ritz method to study the transverse deflection of a rotating orthotropic blade. The transient dynamic responses of rotating pre-twisted shell with isotropic material are presented by Yao *et al.* [10]. They studied the effect of external excitations caused by the aerodynamic pressure which is modeled using the first-order piston theory. Application of the absolute nodal coordinate formulation is examined by Chen *et al.* [11] for studying the transient dynamics of a rotating plate. A study on a rotating blade with isotropic material and the initial geometric imperfection is conducted by Gu *et al.* [12]. They used the Rayleigh-Ritz method with algebraic polynomial functions and examined the effects of different parameters on the free vibration. According to the Kirchhoff plate and the modified couple stress theories, the transient response of the rotating rectangular cantilever microplates is analyzed by Fang *et al.* [13]. For a more complete review of the literature, readers are referred to references [14-16]. Recently, an understanding of the vibration behavior of rotating blades was carried out by Xiang *et al.* [17]. By applying the meshless kp-Ritz method, they also studied lay-up optimization of rotating laminated composite shells.

This paper studies the vibration of cantilever plates under rotating conditions with a stagger angle. An orthotropic material is selected for the analysis. Two different analytical solution procedures, extended Galerkin method (EGM) and extended Kantorovich method (EKM), have been used to evaluate the dynamics of the system. EGM is a weighted residual method and EKM reduces the partial differential equation (PDE) to ordinary differential equations (ODE). The study is divided into three parts. First, using two types of trial functions, the time response of the system has been investigated. Also, by employing a different number of admissible functions in each direction, the convergence of the time response has been examined. Actually, in this part, the effects of paying attention to assumed modes and their orthogonal conditions are discussed in more detail. Second, the notable features in the dynamic characteristics of rotating orthotropic plates are revealed through a parametric study showing the effects of degree of orthotropy,

setting angle, rotational speed, and hub radius ratio. Finally, the forced response of rotating plates subjected to a concentrated and distributed excitations is investigated.

The rest of this paper is structured as follows. In Section 2, the governing equations, as well as boundary conditions, are provided. Afterward, the selected methods for the solution of the problem are explained. Section 3 contains the results. The accuracy of approaches is evaluated. The time response of the rotating plate is discussed in details and then, the natural frequencies of plates with various dimensionless parameters are reported and discussed. Finally, conclusions are drawn in Section 4.

2. Structural model

Consider a thin plate of orthotropic material with density ρ and material constants Q_{ij} , mounted with setting angle φ on a hub with radius R , rotating with constant angular speed Ω as shown in Fig. 1. The Cartesian coordinate system and dimensions have been depicted in the figure in which l is length, b , h denote width and thickness respectively, and x , y , z are coordinate axes.

Taking into account the centrifugal and Coriolis forces effect and according to the following parameters and non-dimensionalized variables,

$$I_0 = \rho h, \quad I_2 = \rho \frac{h^3}{12}, \quad N'_x = I_0 \int_x^l \Omega^2 (R+x) dx, \quad N'_y = I_0 \int_y^{\pm b/2} \Omega^2 \cos^2 \varphi y dy$$

$$A_{ij} = hQ_{ij}, \quad D_{ij} = \frac{h^3}{12} Q_{ij} \quad i, j = 1, 2, 6 \tag{1}$$

$$\hat{x} = \frac{x}{l}, \quad \hat{y} = \frac{y}{b}, \quad \hat{u} = \frac{u}{l}, \quad \hat{v} = \frac{v}{l}, \quad \hat{w} = \frac{w}{l}, \quad C = \frac{l}{b}, \quad \eta = \frac{l}{h}, \quad T = l \sqrt{\frac{I_0}{A_{11}}}, \quad \hat{t} = \frac{t}{T}, \quad \bar{\Omega} = \Omega T, \quad \bar{\omega} = \omega T$$

$$a_{22} = \frac{A_{22}}{A_{11}}, \quad a_{12} = \frac{A_{12}}{A_{11}}, \quad a_{66} = \frac{A_{66}}{A_{11}}, \quad d_{11} = \frac{D_{11}}{A_{11}l^2}, \quad d_{12} = \frac{D_{12}}{A_{11}b^2}$$

$$d_{22} = \frac{D_{22}}{A_{11}b^2}, \quad d_{66} = \frac{D_{66}}{A_{11}b^2}, \quad I_{22} = \frac{I_2}{I_0l^2}, \quad I'_{22} = C^2 I_{22}, \quad r = \frac{R}{l} \tag{2}$$

the dimensionless governing differential equations are written as follows[15]:

$$\frac{\partial^2 u}{\partial x^2} + C(a_{12} + a_{66}) \frac{\partial^2 v}{\partial x \partial y} + C^2 a_{66} \frac{\partial^2 u}{\partial y^2} - 2\bar{\Omega} \sin \varphi \frac{\partial w}{\partial t} + \bar{\Omega}^2 (r + x + u) + 2\bar{\Omega} \cos \varphi \frac{\partial v}{\partial t} - \frac{\partial^2 u}{\partial t^2} = 0 \tag{3}$$

$$C^2 a_{22} \frac{\partial^2 v}{\partial y^2} + C(a_{12} + a_{66}) \frac{\partial^2 u}{\partial x \partial y} + a_{66} \frac{\partial^2 v}{\partial x^2} + \bar{\Omega}^2 \cos^2 \varphi \left(\frac{y}{C} + v \right) - 2\bar{\Omega} \cos \varphi \frac{\partial u}{\partial t} - \bar{\Omega}^2 \sin \varphi \cos \varphi w - \frac{\partial^2 v}{\partial t^2} = 0 \tag{4}$$

$$-d_{11} \frac{\partial^4 w}{\partial x^4} - 2(d_{12} + 2d_{66}) \frac{\partial^4 w}{\partial x^2 \partial y^2} - C^2 d_{22} \frac{\partial^4 w}{\partial y^4} - I_{22} \bar{\Omega}^2 \frac{\partial^2 w}{\partial x^2} - I'_{22} \bar{\Omega}^2 \cos^2 \varphi \frac{\partial^2 w}{\partial y^2} - \bar{\Omega}^2 \sin \varphi \cos \varphi \left(\frac{y}{C} + v \right)$$

$$+ 2\bar{\Omega} \sin \varphi \frac{\partial u}{\partial t} + \bar{\Omega}^2 \sin^2 \varphi w + \frac{\partial \bar{N}'_x}{\partial x} \frac{\partial w}{\partial x} + \bar{N}'_x \frac{\partial^2 w}{\partial x^2} + \frac{\partial \bar{N}'_y}{\partial y} \frac{\partial w}{\partial y} + \bar{N}'_y \frac{\partial^2 w}{\partial y^2} - \frac{\partial^2 w}{\partial t^2} + q_3 = 0 \tag{5}$$

Where q_3 is lateral distributed load and hats (^) are eliminated from all the quantities. The associated dimensionless boundary conditions are:

$$u = v = w = \partial w / \partial x = 0 \quad @ \quad x = 0. \quad (6)$$

$$M_x = M_{xy} = N_x = N_{xy} = Q_x = 0 \quad @ \quad x = 0 \quad (7)$$

$$M_y = M_{xy} = N_y = N_{xy} = Q_y = 0 \quad @ \quad y = \pm 1/2. \quad (8)$$

In these equations, u , v and w are the displacement components in x , y , z directions, respectively. Furthermore, in this study, the influence of dynamic loads on the stress is investigated. The strain-stress relations can be computed by:

$$\begin{aligned} \bar{\sigma}_x &= Q_{11}\epsilon_x + Q_{12}\epsilon_y \\ \bar{\sigma}_y &= Q_{22}\epsilon_y + Q_{12}\epsilon_x \\ \bar{\sigma}_{xy} &= Q_{66}\gamma_{xy} \end{aligned} \quad (9)$$

The dimensionless stresses are expressed as:

$$\begin{aligned} \sigma_x &= 12z\eta^2 \left(d_{11} \frac{\partial^2 w}{\partial x^2} + d_{12} \frac{\partial^2 w}{\partial y^2} \right) \\ \sigma_y &= 12z\eta^2 \left(C^2 d_{22} \frac{\partial^2 w}{\partial y^2} + d_{12} \frac{\partial^2 w}{\partial x^2} \right) \\ \sigma_{xy} &= 24z\eta^2 d_{66} \frac{\partial^2 w}{\partial x \partial y} \end{aligned} \quad (10)$$

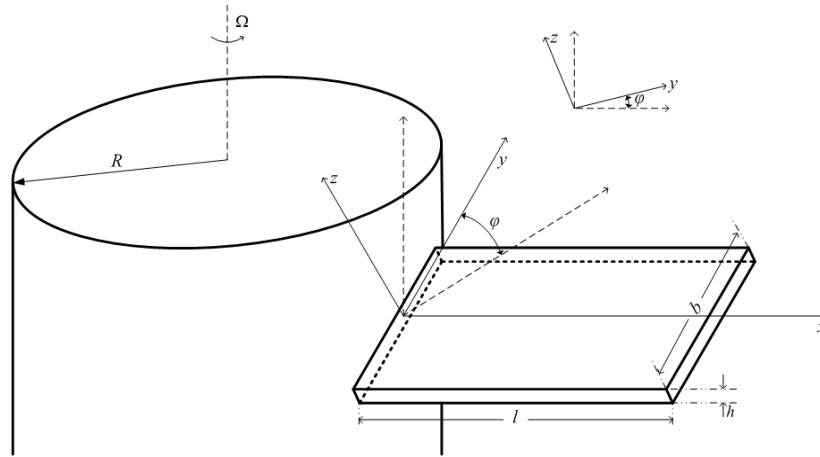


Fig 1. Schematic of the wing model showing local and global coordinate systems.

Various methods for the static and dynamic solutions of engineering complicated problems are available. In the present work, EGM and EKM are employed to solve the vibration problem of a rotating plate.

According to the EGM, the deformation variables are approximated as follows:

$$\begin{aligned}
 u(x, y, t) &= \sum_i \sum_j \chi_i^{(u)}(x) \zeta_j^{(u)}(y) q_{ij}^{(u)}(t) \\
 v(x, y, t) &= \sum_i \sum_j \chi_i^{(v)}(x) \zeta_j^{(v)}(y) q_{ij}^{(v)}(t) \\
 w(x, y, t) &= \sum_i \sum_j \chi_i^{(w)}(x) \zeta_j^{(w)}(y) q_{ij}^{(w)}(t)
 \end{aligned}
 \tag{11}$$

where $\chi_i^{(n)}$, $\zeta_j^{(n)}$ and $q_{ij}^{(n)}$ ($n=u, v, w$) are trial functions and generalized coordinates, respectively. Placing Eq. (11) in the governing equations and minimizing the weighted residuals, the discretized equations can be achieved. Then, the equations can be cast in the state space form.

Another efficient technique, the EKM, is also applied here. The basic concept of the EKM is that the displacements can be approximated as the separable solution forms,

$$\begin{aligned}
 u(x, y, t) &= U(x, y)e^{i\bar{\omega}t} = \xi_1(x)\psi_1(y)e^{i\bar{\omega}t} \\
 v(x, y, t) &= V(x, y)e^{i\bar{\omega}t} = \xi_2(x)\psi_2(y)e^{i\bar{\omega}t} \\
 w(x, y, t) &= W(x, y)e^{i\bar{\omega}t} = \xi_3(x)\psi_3(y)e^{i\bar{\omega}t}
 \end{aligned}
 \tag{12}$$

where the unknown functions of $\xi_i(x)$ and $\psi_i(y)$ should be determined. With the substitution of Eq. (12) into Eqs. (3) – (5) and set of prescribed functions, the solution of the partial differential equations is reduced to an iterative sequential solution of a double system of ordinary differential equations. The iterative manner continues until convergence is achieved to the arbitrary accuracy for the natural frequency. More details about the method are available in references[18, 19].

3. Results

To verify the accuracy of the methods and to investigate the modal characteristics of rotating plates with different stagger angles, hub radius ratio, and aspect ratio at different angular velocities, several dimensionless numerical examples are studied here. The material properties of the orthotropic plate are given as:

$$\nu_{12}\nu_{21} = \nu^2 \ (\nu = 0.3), \ G_{12} = \frac{\sqrt{E_{11}E_{22}}}{2(1 + \sqrt{\nu_{12}\nu_{21}})}
 \tag{13}$$

Table 1 depicts the first four frequency parameters obtained on the basis of EKM and those obtained from EGM for a rotating orthotropic cantilever plate with the hub radius ratio of 0 and 1, respectively. The aspect ratio of the plate is two and the stagger angle is zero ($C=2$ and $\varphi=0$).

It can be seen from Table 1 that the difference between the results of two methods is not significant and the comparisons show close agreement. The maximum and minimum deviation is about 1.9% and 0.09%, respectively.

As mentioned earlier, this study has been divided into two parts. In the first part, the time response of the system has been presented using two kinds of trial functions. The effects of using a different number of mode shapes in each direction have been investigated. In the second part, the influences of dimensionless parameters on the modal characteristics of rotating plates have been discussed.

Figure 2. provides the time response of the rotating isotropic cantilever plate using a different number of trial functions. The plate has a hub radius ratio of 0, the aspect ratio of one, and the stagger angle of $\pi/6$. The type of trial functions is polynomials. As shown in Fig. 2 when the number of functions has been increased from $N=2$ to $N=5$ in each direction, the time response has been changed significantly. Also, there is a small difference in the time responses obtained using 4 and 5 functions in each direction. So, it can be concluded that considering 4 trial functions in each direction is sufficient to determine the time response of the system.

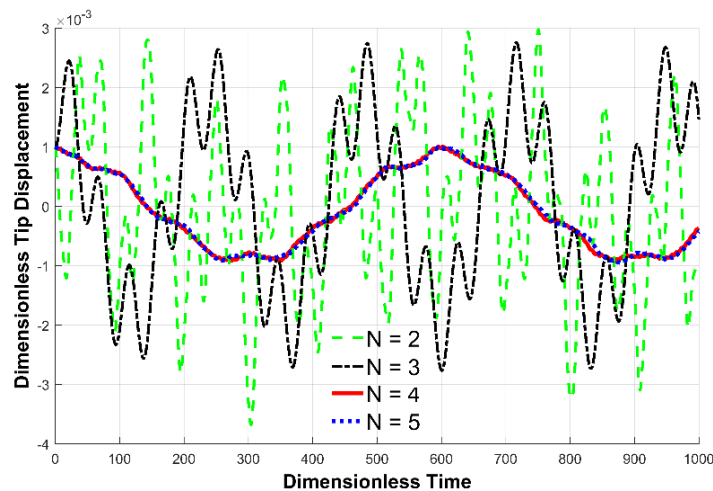


Fig 2. Time response of the rotating isotropic cantilever plate using polynomials trial functions.

The time response of the system using a different number of plate characteristic functions has been presented in Fig.3. From Fig. 3 we can see that increasing the number of functions, does not have a significant effect on the time response. So, it can be deduced that considering two trial functions is well enough. Also, it can be seen from Fig 2. and Fig 3. that the rate of convergence using plate characteristic functions is much faster than using polynomials functions. Figure 4. compares the time response of the rotating isotropic cantilever plate obtained from using different kinds of trial functions. It is observed that using plate characteristic functions leads to a smoother time response which seems to be more realistic.

Table 1. Non-dimensional frequency parameter, $\bar{\omega} = \omega l \sqrt{I_0 / A_{11}}$, for rotating rectangular cantilever plate.

		C=2, $\eta = 0.01$							
Material	Mode	r=0				r=1			
		$\bar{\Omega} = \Omega l^2 \sqrt{I_0 / D_{11}} = 1$		$\bar{\Omega} = \Omega l^2 \sqrt{I_0 / D_{11}} = 2$		$\bar{\Omega} = \Omega l^2 \sqrt{I_0 / D_{11}} = 1$		$\bar{\Omega} = \Omega l^2 \sqrt{I_0 / D_{11}} = 2$	
		EKM	EGM	EKM	EGM	EKM	EGM	EKM	EGM
$E_{22}/E_{11}=0.4$	1	0.0106054	0.0104522	0.0119244	0.0117932	0.0112047	0.0110613	0.0139376	0.0138295
	2	0.0356335	0.0355464	0.0363616	0.0362760	0.0358218	0.0357349	0.0370932	0.0370081
	3	0.0635441	0.0624019	0.0648112	0.0636836	0.0641101	0.0629729	0.0670010	0.0658909
	4	0.119228	0.1183979	0.1200571	0.1192289	0.11956321	0.1187327	0.1213787	0.1205503
$E_{22}/E_{11}=1$	1	0.010603	0.0104219	0.01192315	0.0117668	0.0112032	0.0110329	0.0139365	0.0138076
	2	0.043010	0.0429442	0.0436153	0.0435503	0.0431685	0.0431028	0.0442362	0.0441715
	3	0.063445	0.0623246	0.0647155	0.0636094	0.0640128	0.0628977	0.0669094	0.0658246
	4	0.140027	0.1393551	0.1407483	0.1400759	0.1403232	0.1396500	0.1419173	0.1412430
$E_{22}/E_{11}=2.5$	1	0.010602	0.0103911	0.0119221	0.0117399	0.0112021	0.0110040	0.0139357	0.0137852
	2	0.052354	0.0523051	0.0528528	0.0528039	0.0524864	0.0524371	0.0533728	0.0533242
	3	0.063345	0.0622186	0.0646181	0.0635064	0.0639138	0.0627933	0.0668162	0.0657277
	4	0.166708	0.1662052	0.1673263	0.1668225	0.1669654	0.1664614	0.1683451	0.1678392

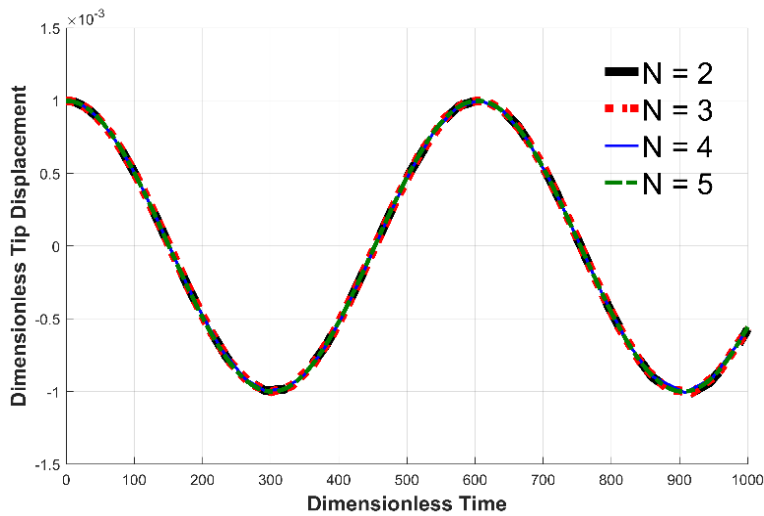


Fig 3. Time response of the rotating isotropic cantilever plate using plate characteristics functions.

For better interpretation as well as a detailed study of the given time responses, the power spectrum plots corresponding to Fig. 4 are demonstrated in Fig 5 and Fig 6. Fig. 5 is related to the power spectrum of the first mode of the system when the plate characteristic function is used. As can be seen, Fig. 5 just shows the first frequency which is equal to 0.01046. Actually, it can be deduced that because of using a perfect trial function in the solution procedure and establishing the orthogonality condition between modes, the generalized coordinates are decomposed. Therefore, the first-order mode is only stimulated.

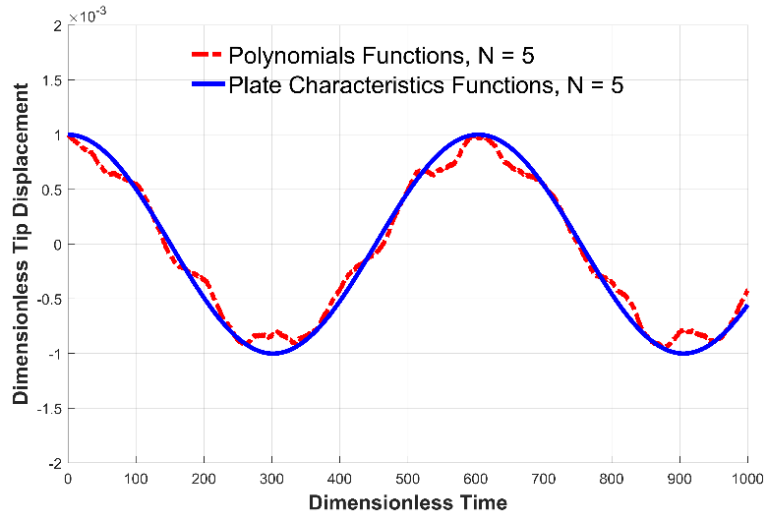


Fig 4. Comparison of time response of the rotating isotropic cantilever plate obtained from different trial functions.

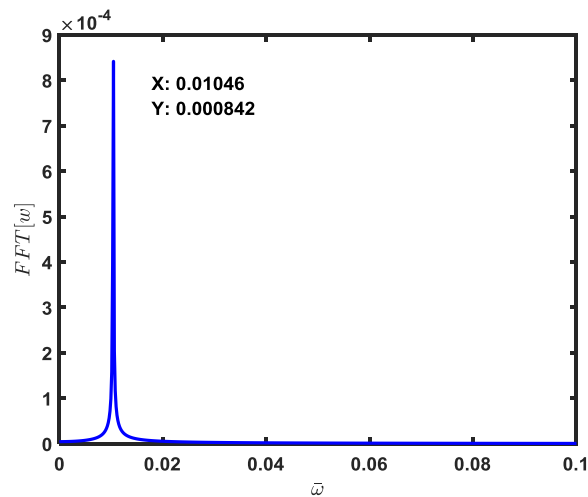


Fig 5. The frequency spectrum related to the time response obtained by plate characteristic functions.

Fig. 6 illustrates the power spectrum associated with the time history curve of plate oscillation when the polynomials are selected as an admissible function. This figure reveals the incidence of three frequencies, while one of them has considerable power in comparison with others. The considerable power is related to the frequency of the first bending mode and as can be observed, it is equal to the frequency of the previous case. Two other frequencies which are appeared in the diagram are higher bending modes. Based on the existence of the higher modes in the frequency spectrum, it can be perceived that when the first mode is excited, there is a coupling between modes. Therefore, it is inferred that due to the loss of orthogonality conditions in the assumed modes, this coupling exists.

From the above results, it is concluded that using suitable as well as sufficient numbers of trial functions is essential and the consequence of not paying attention to that can lead to the approximation results in poor accuracy.

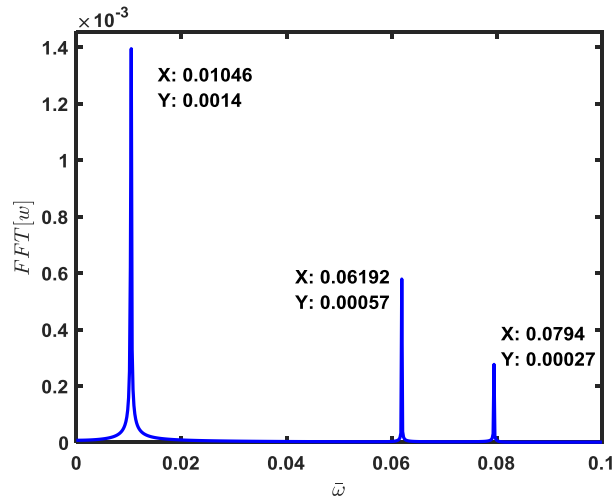


Fig 6. The frequency spectrum related to. the time response obtained by polynomials functions.

To focus on the critical effects of parameters on the modal characteristics due to the rotation, Campbell diagrams of the problem are drawn. Figures 7 and 8 compare the first three non-dimensional frequencies. From these figures, one can see that for $C=1$, the curves of $E_{22} / E_{11} = 0.4$ have uniform trends but for $E_{22} / E_{11} = 1$ and 2.5, the slope of variations at a certain speed is changed. It shows that with the increase of the stiffness ratio, there is the possibility of the appearance of “veering” in these cases. At $C=2$, $r=0$ and for various angles, all curves of the different stiffness ratios overlap. Such conditions can indicate that there is a spanwise bending frequency. With increasing hub radius ratio, the curves related to stiffness ratio equal to 0.4 exhibit different trends at a certain speed. These changes demonstrate that, at this speed, the increase of hub radius ratio causes the occurrence of “veering”.

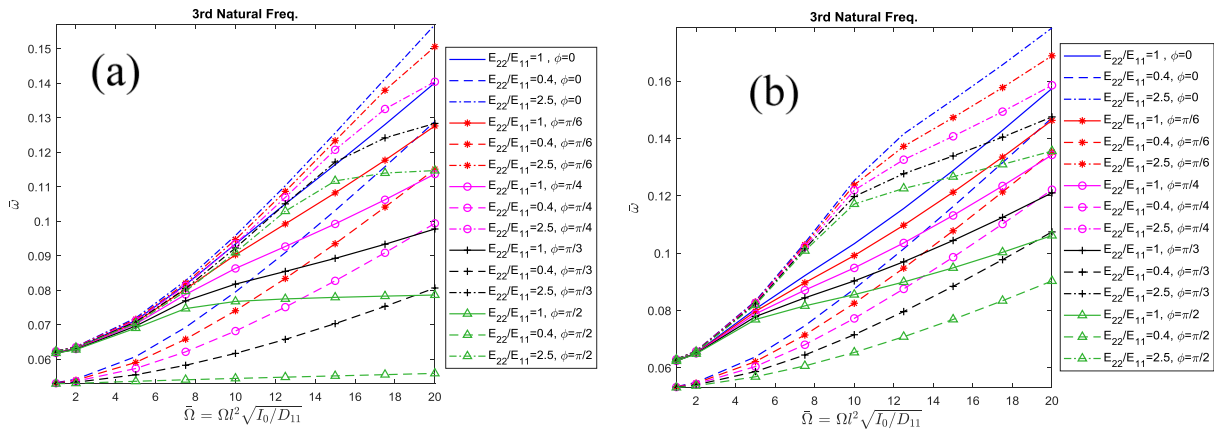


Fig 7. The relative changes in the third natural frequency, $\bar{\omega} = \omega \sqrt{I_0 / A_{11}}$, with varying rotational speed of a rectangular plate, $C=1$, (a) $r=0$ and (b) $r=1$.

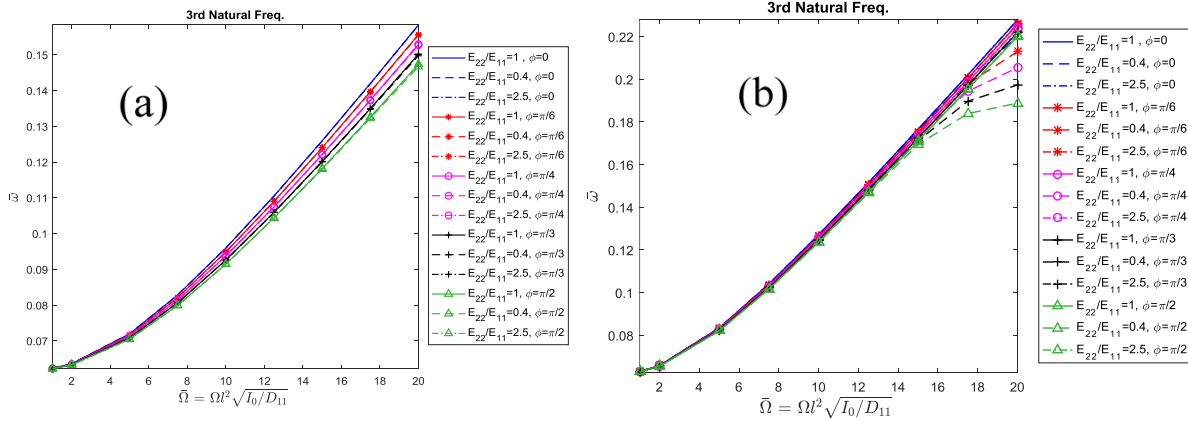


Fig 8. The relative changes in the third natural frequency, $\bar{\omega} = \omega \sqrt{I_0 / A_{11}}$, with varying rotational speed of a rectangular plate, $C=2$, (a) $r=0$ and (b) $r=1$.

The Campbell diagram corresponding to the frequencies of first chordwise bending mode is presented in Fig.9 (a), for aspect ratio $C=1$ and $\varphi=0$. Results indicated that for a given hub radius ratio, with increasing rotational speed, the curves related to different stiffness ratios have converged and the convergence rate is increased as the hub radius ratio increases.

To consider the effect of the stagger angle on the first chordwise bending mode, Fig.9 (b) is drawn. The aspect ratio of the plate is 1 and $r=1$. As the angular speed increases, the convergence between two stiffness ratios 0.4 and 2.5 in the different stagger angles is also observed. In Fig.10 (a) and (b), the loci of the natural frequencies of second torsion mode are displayed for rotating plates with an aspect ratio 2. From this figure, it can be clearly seen that for a given hub radius ratio and/or stagger angle, by increasing the rotation speed, the curves of different stiffness ratios are approaching each other. In this mode, increasing the hub radius ratio increase the convergence, whereas the increase of stagger angle insignificantly decreases it. This means that the plate with a lower stiffness ratio is more affected by the centrifugal inertia forces.

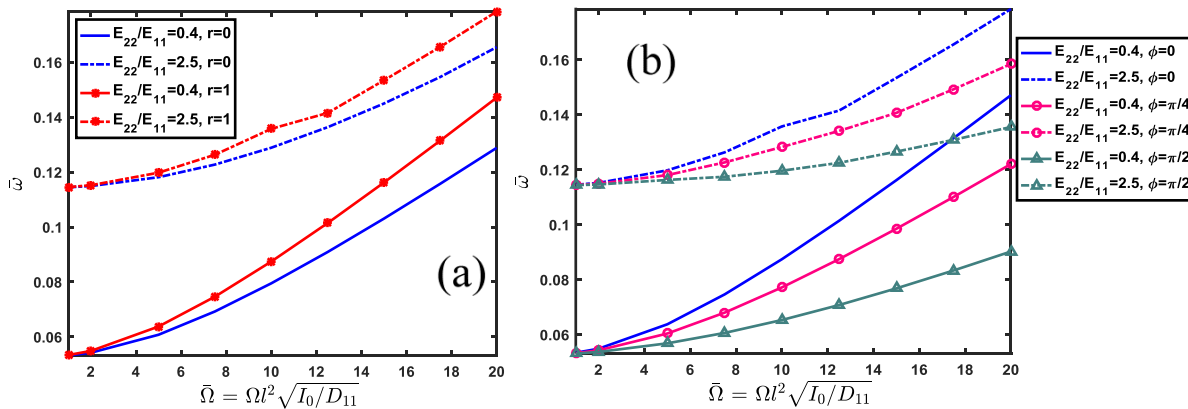


Fig 9. Variations of the first chordwise bending mode versus dimensionless rotational speed corresponding to (a) $C=1, \varphi=0$ and (b) $C=1, r=1$.

Besides forces due to the rotation influence, a rotating system can be subjected to some type of external excitation that acts on the blade, such as aero forces from the gas flow. This unsteady

aero force over the blade surface can affect the response of the system dramatically. Therefore, the last part of this paper is devoted to studying the forced response. In this regard, two types of forces, i.e. concentrated load and distribution force, are applied to determine the dynamic responses of the structure. The forced responses are investigated while only the dynamic forces are considered.

To verify this part of the study, static analysis of a stationary isotropic cantilever plate under the action of different load conditions is performed. The values of the non-dimensional transverse deflections and bending moments for a square plate under a concentrated load (P) at $(l, -b/4)$ are shown in Tables 2 and 3. The results related to the plate subjected to a uniform load (q_3) are demonstrated in Tables 4 and 5. The calculated results for the specific locations in these tables are compared with Ref. [20]. There is a good agreement between the results obtained from the two methods.

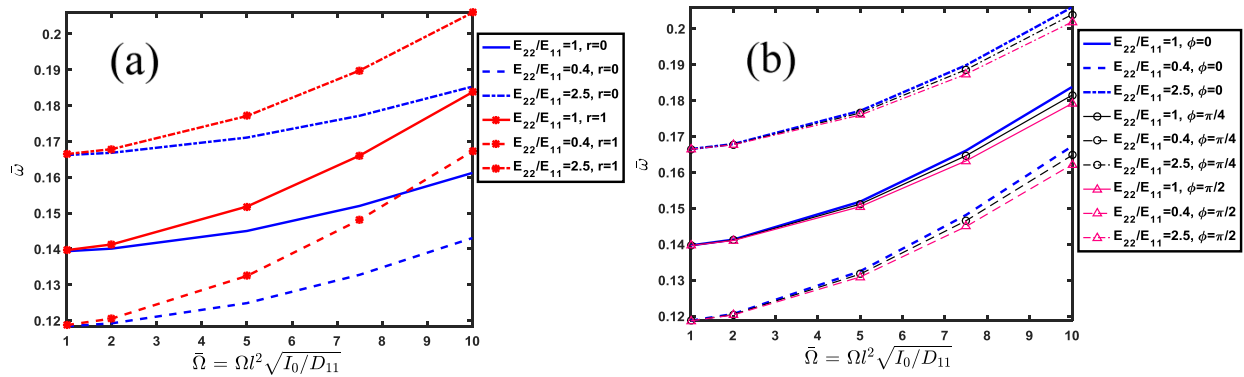


Fig 10. The relative changes in the second torsion mode with varying rotational speed; (a) $C=2, \varphi=0$ (b) $C=2, r=1$.

Table 2. Deflections of a stationary isotropic cantilever plate under a concentrated load at $(l, -b/4)$.

$D_{11}w / Pl^2, C=1, 1/\eta = 0.01$										
	$x = 0$		$x = l/4$		$x = l/2$		$x = 3l/4$		$x = l$	
	Present	Ref. 20	Present	Ref. 20	Present	Ref. 20	Present	Ref. 20	Present	Ref. 20
$y = +b/2$	0	0	0.01553	0.0157	0.0729	0.0733	0.1627	0.163	0.2693	0.268
$y = -b/2$	0	0	0.03239	0.0323	0.1248	0.125	0.2558	0.256	0.4040	0.402

Table 3. Deflections of the free edge $x=l$ and bending moments of clamped edge $x=0$ for a stationary isotropic cantilever plate under a concentrated load at $(l, -b/4)$.

$D_{11}w / Pl^2, M_x / P, C=1, 1/\eta = 0.01$										
	$y = -b/2$		$y = -b/4$		$y = 0$		$y = +b/4$		$y = +b/2$	
	Present	Ref. [20]	Present	Ref. [20]	Present	Ref. [20]	Present	Ref. [20]	Present	Ref. [20]
$w(l,y)$	0.2693	0.268	0.03059	0.305	0.3483	0.346	0.3871	0.386	0.4040	0.402
$M_x(0,y)$	0.0772	-	0.9034	0.935	1.1194	1.09	1.2425	1.26	0.5817	-

Table 4. Deflections of a stationary isotropic cantilever plate under uniform load.

		$D_{11}w / q_3 l^4, C=1, 1/\eta = 0.01$									
		$x = 0$		$x = l/4$		$x = l/2$		$x = 3l/4$		$x = l$	
		Present	Ref. [20]	Present	Ref. [20]	Present	Ref. [20]	Present	Ref. [20]	Present	Ref. [20]
$y = +b/2$	0	0	0	0.01178	0.0117	0.0432	0.0433	0.0839	0.0841	0.1271	0.127
$y = -b/2$	0	0	0	0.01178	0.0117	0.0432	0.0433	0.0839	0.0841	0.1271	0.127

Table 5. Deflections of the free edge $x=l$ and bending moments of clamped edge $x=0$ for a stationary isotropic cantilever plate under uniform load.

		$D_{11}w / q_3 l^4, M_x / q_3 l^2, C=1, 1/\eta = 0.01$									
		$y = -b/2$		$y = -b/4$		$y = 0$		$y = +b/4$		$y = +b/2$	
		Present	Ref. [20]	Present	Ref. [20]	Present	Ref. [20]	Present	Ref. [20]	Present	Ref. [20]
$w(l,y)$	0.1271	0.127	0.1285	0.129	0.1290	0.129	0.1285	0.129	0.1271	0.127	
$M_x(0,y)$	0.2059	-	0.5226	0.530	0.5392	0.531	0.5526	0.530	0.2059	-	

Furthermore, the non-dimensional deflections and bending moments of the stationary cantilever plate with aspect ratios 0.5 and 1 under uniform load are reported in Table 6. For comparison, the table also includes the works done by Wang *et al.*[21] and Lin *et al.* [22]. The results are in good agreement with the calculations presented in references.

In the forced vibration analysis, a rotating isotropic plate is used at zero stagger angle and with hub radius ratio zero. In the first case study, a rotating square plate at rotational speed $\bar{\Omega} = 10$ is under a 0.2 N point force which is located at $(l, -b/4)$, normal to the plate surface. The von Mises stress is effective stress which can be used to predict a lifetime. Therefore, the Von Mises stresses are computed under the influence of dynamic loads. To analyse Von Mises stress at different frequencies, first, the displacement response for a specific frequency is obtained, and based on that, the stress fields are calculated. In other words, the displacement of the plate at one of the frequencies is computed and then, the other quantities are explored. The contours of non-dimensional Von Mises stress over the top surface of the plate are displayed in Fig.11 at the first four frequencies. In the different modes, the locations of the minimum and maximum stresses are seen in the figures. Because the third and fourth frequencies are approaching each other, most parts of the stress contours associated with them almost have the same areas. Fig.12 presents Von Mises stress contours for force excitations at an intermediate frequency of two consecutive modes. As can be appreciated from this figure, the intermediate frequencies give asymmetric contours which are a combination of two modes.

Table 6. Deflections and bending moments of a stationary cantilever plate under uniform load.

E ₂₂ /E ₁₁ =1, 1/η = 0.01									
	C=1/2,				C=1,				
	D ₁₁ w / q ₃ l ⁴		M _x / q ₃ l ²		D ₁₁ w / q ₃ l ⁴		M _x / q ₃ l ²		
	(l, 0)	(l, b/2)	(0, 0)	(0, b/2)	(l, 0)	(l, b/2)	(0, 0)	(0, b/2)	
Present	0.1277	0.1242	0.5344	0.2457	Present	0.1290	0.1271	0.5392	0.2455
Ref. 21	0.1284	0.1253	0.5147	0.3564	Ref. 22	0.1291	0.1272	0.5355	0.2431

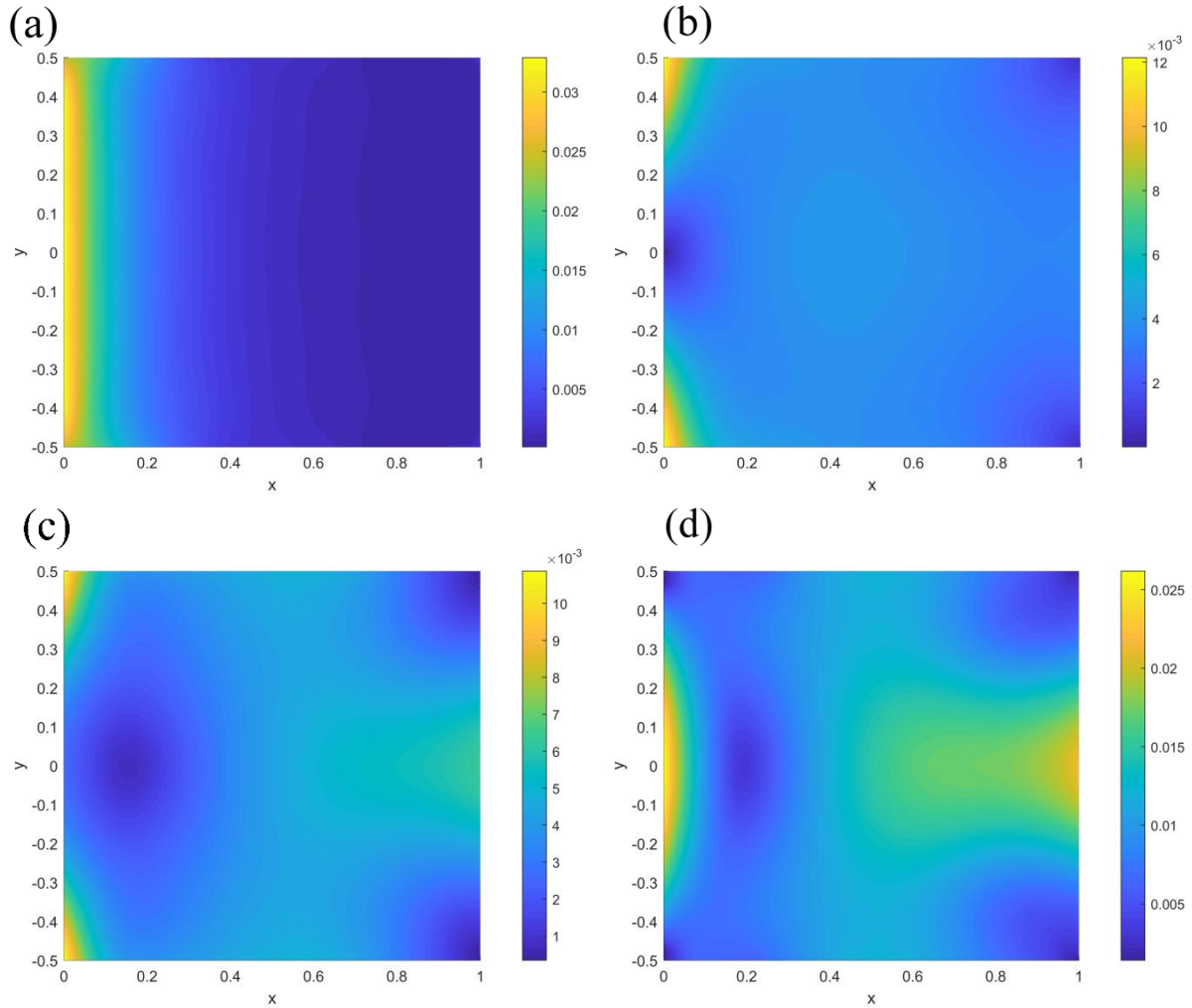


Fig 11. Von Mises stress over the top surface of the rotating square plate under point load at (a) the first mode, (b) the second mode, (c) the third mode, (d) the fourth mode.

(a)

(b)

(c)

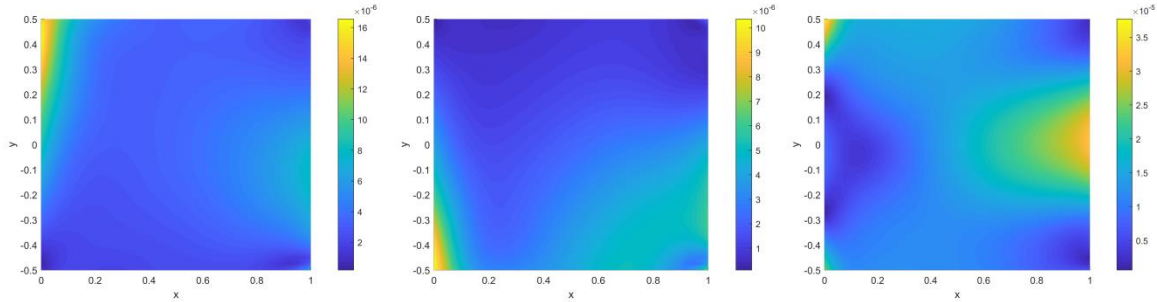


Fig 12. Von Mises stress over the top surface of the rotating square plate under point load at (a) $\bar{\omega} = 0.04$, (b) $\bar{\omega} = 0.07$, (c) $\bar{\omega} = 0.09$.

In the next case study, the rotating square plate is subjected to a uniform distributed pressure loading on the plate surface with the purpose of the aero force simulation. The rotational speed of the plate is set to 10 and the value of the force is $0.2/lb\ Nm^{-2}$. Von Mises stress contours for this case are plotted in Figs.13 to 16. Non-dimensional stress components of the plate ($\bar{\sigma}_x$ and $\bar{\sigma}_y$), along the lines $y=0$ and $x=0$, are also included in the figures. The excitation frequencies of the dynamic loading are chosen equal to the first four natural frequencies of the system. The first to fourth modes of the rotating plate are 1 bending, 1 torsion, 2 bending and 1 chordwise bending modes, respectively. It can be seen from Fig. 13 that the distribution of stresses along the clamped edge is almost uniform but in the two comers of the clamped edge, there is an abrupt decrease.

In Fig. 14, according to the stress distribution of the clamped edge as well as the lower values of the stresses, it is inferred that the second mode is disappeared. The reason for this happening is due to applying a uniform load and hence, the torsion frequency is suppressed.

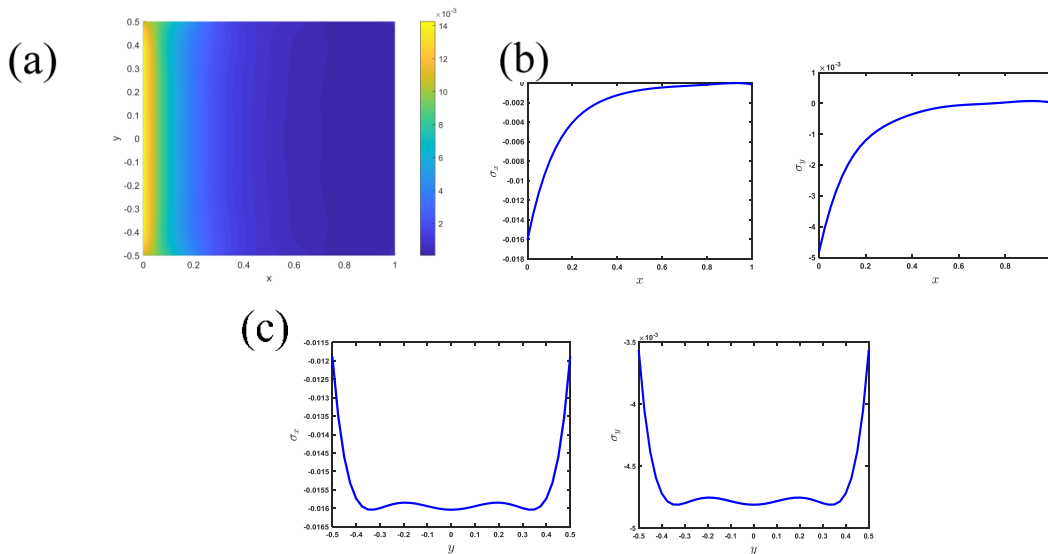


Fig 13. (a) Von Mises stress and stress components along (b) $y=0$ and (c) $x=0$ over the top surface of the rotating square plate under distributed load at the first mode.

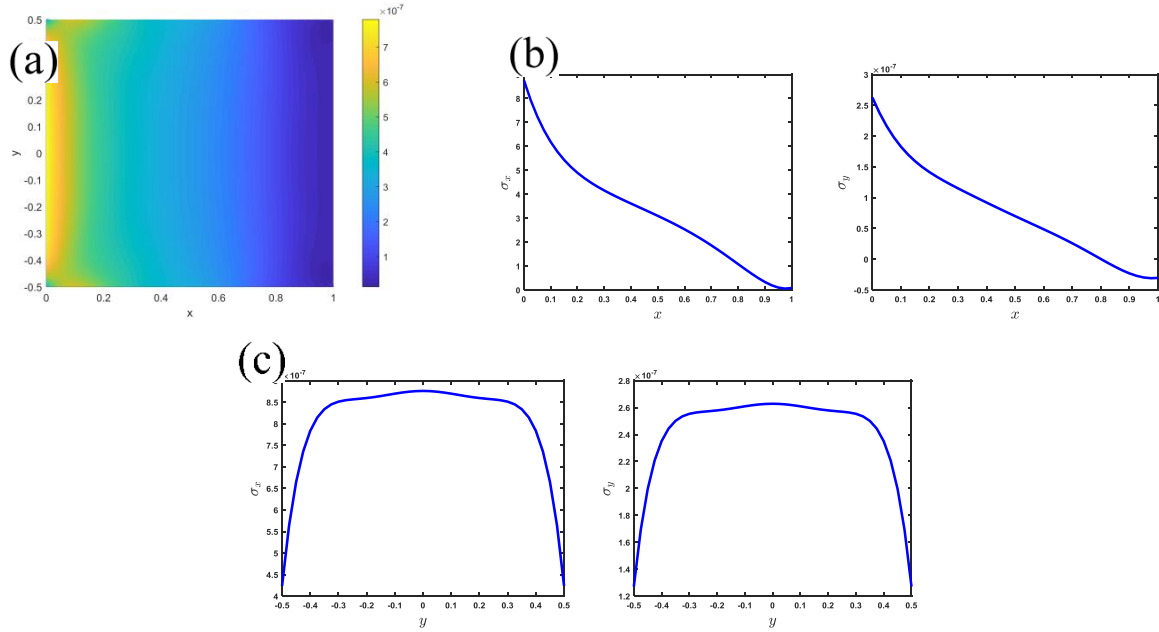


Fig 14. (a) Von Mises stress and stress components along (b) $y=0$ and (c) $x=0$ over the top surface of the rotating square plate under distributed load at the second mode.

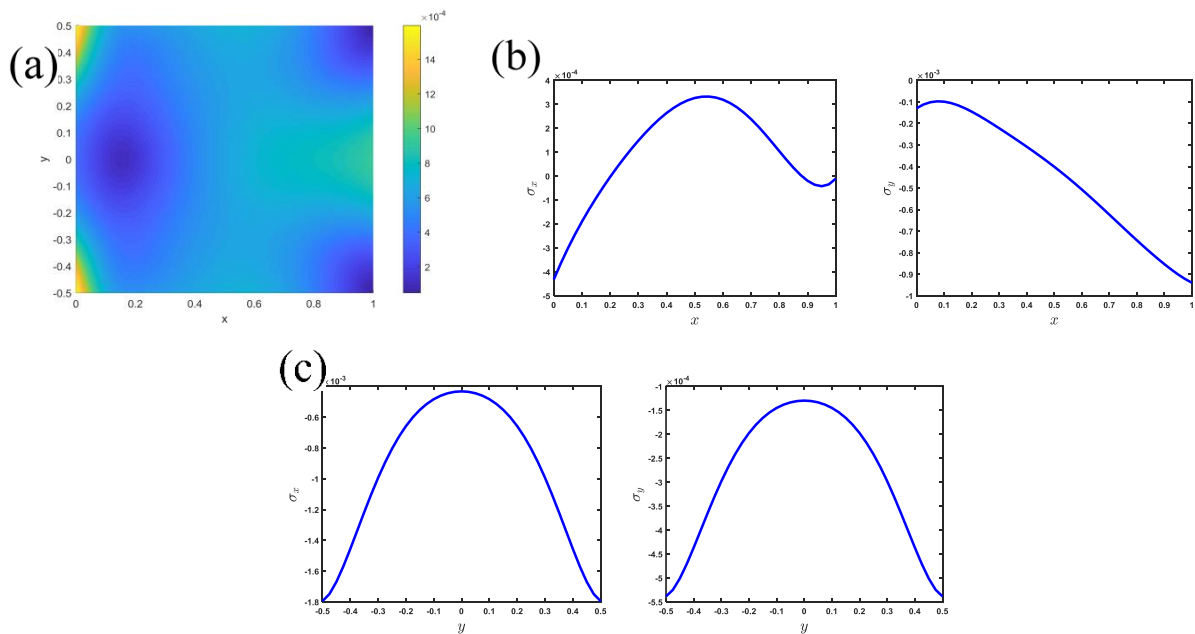


Fig 15. (a) Von Mises stress and stress components along (b) $y=0$ and (c) $x=0$ over the top surface of the rotating square plate under distributed load at the third mode.

Based on Fig. 15 and Fig. 16, it is clear that by applying distributed load the same as point force, the response curves corresponding to the third and fourth modes are similar. As can be seen, in both modes, the increase and decrease variations of stresses along the clamped edge, from one corner to another, are smooth and the curves related to the third and fourth modes are concave downward and concave upward, respectively.

For investigating the effect of rotational speed on the Von Mises stress, Fig. 17 is plotted. Fig. 17 illustrates the variations of Von Mises stresses along the centerline $y=0$ for different rotational speeds. From this figure, it is found that the minimum Von Mises stresses occurred at the tip of the plate. It can be noticed that with increasing the rotation speed, the values of stresses near the tip of plate decrease and converge to zero.

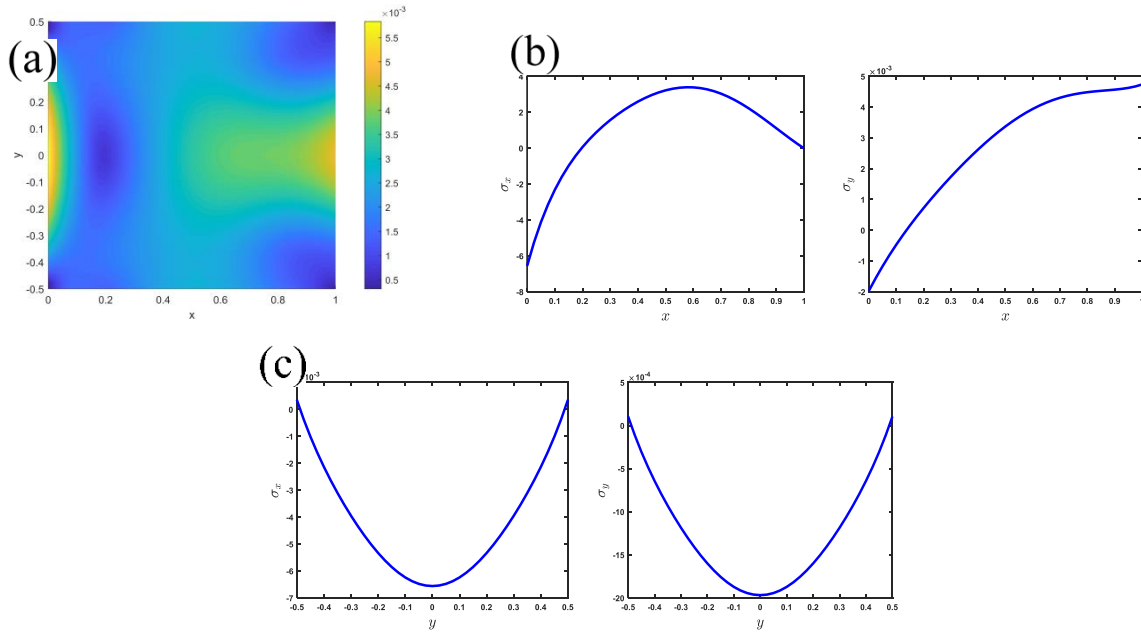


Fig 16. (a) Von Mises stress and stress components along (b) $y=0$ and (c) $x=0$ over the top surface of the rotating square plate under distributed load at the fourth mode.

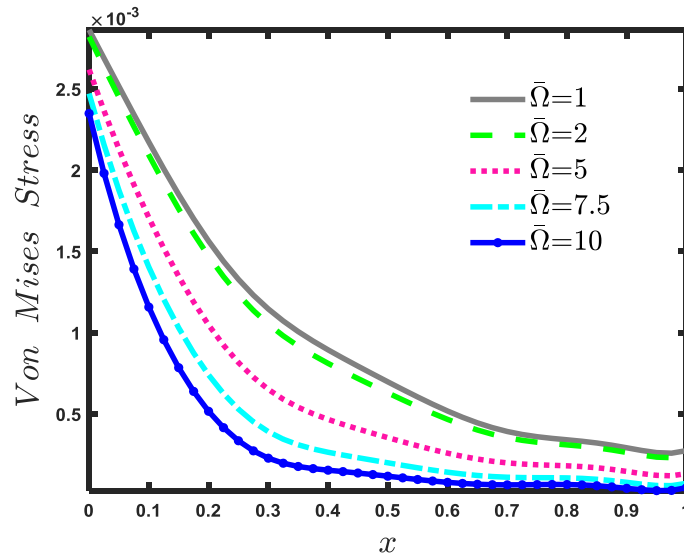


Fig 17. Von Mises stress of the rotating plate along the centerline $(x,0)$ with increasing the rotational speed.

4. Conclusion

In this paper, the time response and natural frequency of free vibration were investigated for a rotating orthotropic cantilever plate with different stagger angles, aspect ratios, hub radius ratios and angular speeds. An extended Galerkin method (EGM) along with extended Kantorovich method (EKM) was utilized to solve the equations of motion. It has been demonstrated that the type of trial functions has a significant effect on the sufficient number of functions needed to obtain accurate results. The number of sufficient trial functions has been decreased significantly when polynomials have been replaced by products of plate characteristic functions. Increasing the quality of the trial functions could lead to decreasing the number of mode shapes and having a harmonic response. However, the polynomials functions are much simpler than plate characteristic functions and this could end up making them more applicable for engineering problems when there is a constraint to choose the trial functions. Actually, it can be said that using suitable trial functions is important and also, based on the kind of admissible function, a sufficient number of functions should be selected for the solution procedure. Not paying attention to that could lead to obtaining the results from approximation methods with poor accuracy. Indeed, the proper choice of assumed modes can guarantee the convergence speed and accuracy of an approximate solution. The results of the several numerical examples reveal that with the variation of hub radius ratio, veering can occur between the eigenvalues loci. Thus, it must be emphasized that the hub radius has an important role in rotating machinery designs. The effects of the system configuration on the frequencies of the chordwise bending and second torsion modes were also studied. It was demonstrated that in those modes, the plate with a lower stiffness ratio has a higher centrifugal stiffening rate. Moreover, it is noted that the influence of the hub radius ratio on the centrifugal stiffening is more significant in comparison to that of the stagger angle. The last part of this paper was devoted to present the response of rotating plates subjected to forced vibration. Two types of point and distribution forces were applied to excite the system and also, the effect of rotational speed on Von Mises stress was evaluated.

References

- [1] M.A. Dokainish, S. Rawtani, Vibration analysis of rotating cantilever plates, *International Journal for Numerical Methods in Engineering*, 3 (1971) 233-248.
- [2] J.T.-S. Wang, D. Shaw, O. Mahrenholtz, Vibration of rotating rectangular plates, *Journal of Sound and vibration*, 112 (1987) 455-468.
- [3] J.S. Rao, K. Gupta, Free vibrations of rotating small aspect ratio pretwisted blades, *Mechanism and Machine Theory*, 22 (1987) 159-167.
- [4] J. Sun, L. Kari, I.L. Arteaga, A dynamic rotating blade model at an arbitrary stagger angle based on classical plate theory and the Hamilton's principle, *Journal of Sound and Vibration*, 332 (2013) 1355-1371.
- [5] S.K. Sinha, K.E. Turner, Natural frequencies of a pre-twisted blade in a centrifugal force field, *Journal of Sound and Vibration*, 330 (2011) 2655-2681.
- [6] H.H. Yoo, S.K. Kim, Free vibration analysis of rotating cantilever plates, *AIAA journal*, 40 (2002) 2188-2196.
- [7] H.H. Yoo, S.K. Kim, D.J. Inman, Modal analysis of rotating composite cantilever plates, *Journal of sound and vibration*, 258 (2002) 233-246.
- [8] L. Li, D.G. Zhang, Free vibration analysis of rotating functionally graded rectangular plates, *Composite Structures*, 136 (2016) 493-504.
- [9] S.K. Sinha, R.P. Zylka, Vibration analysis of composite airfoil blade using orthotropic thin shell bending theory, *International Journal of Mechanical Sciences*, 121 (2017) 90-105.
- [10] M. Yao, Y. Niu, Y. Hao, Nonlinear dynamic responses of rotating pretwisted cylindrical shells, *Nonlinear Dynamics*, 95 (2019) 151-174.

- [11] Y. Chen, D. Zhang, L. Li, Dynamics analysis of a rotating plate with a setting angle by using the absolute nodal coordinate formulation, *European Journal of Mechanics-A/Solids*, 74 (2019) 257-271.
- [12] X.J. Gu, Y.X. Hao, W. Zhang, L.T. Liu, J. Chen, Free vibration of rotating cantilever pre-twisted panel with initial exponential function type geometric imperfection, *Applied Mathematical Modelling*, 68 (2019) 327-352.
- [13] J. Fang, H. Wang, X. Zhang, On size-dependent dynamic behavior of rotating functionally graded Kirchhoff microplates, *International Journal of Mechanical Sciences*, 152 (2019) 34-50.
- [14] H. Rostami, A.R. Ranji, F. Bakhtiari-Nejad, Free in-plane vibration analysis of rotating rectangular orthotropic cantilever plates, *International Journal of Mechanical Sciences*, 115 (2016) 438-456.
- [15] H. Rostami, A.R. Ranji, F. Bakhtiari-Nejad, Vibration characteristics of rotating orthotropic cantilever plates using analytical approaches: a comprehensive parametric study, *Archive of Applied Mechanics*, 88 (2018) 481-502.
- [16] H. Rostami, F. Bakhtiari-Nejad, A.R. Ranji, Vibration of the rotating rectangular orthotropic Mindlin plates with an arbitrary stagger angle, *Journal of Vibration and Control*, 25 (2019) 1194-1209.
- [17] R. Xiang, Z.-Z. Pan, H. Ouyang, L.-W. Zhang, A study of the vibration and lay-up optimization of rotating cross-ply laminated nanocomposite blades, *Composite Structures*, 235 (2020) 111775.
- [18] A.R. Ranji, H.R. Hoseynabadi, A semi-analytical technique for bending analysis of cylindrical panels with general loading and boundary conditions, *Journal of mechanical science and technology*, 26 (2012) 1711-1718.
- [19] A.R. Ranji, H.R. Hoseynabadi, A semi-analytical solution for forced vibrations response of rectangular orthotropic plates with various boundary conditions, *Journal of Mechanical Science and Technology*, 24 (2010) 357-364.
- [20] B. Tian, Y. Zhong, R. Li, Analytic bending solutions of rectangular cantilever thin plates, *Archives of Civil and Mechanical Engineering*, 11 (2011) 1043-1052.
- [21] X. Wang, Y.L. Wang, R.B. Chen, Static and free vibrational analysis of rectangular plates by the differential quadrature element method, *Communications in Numerical Methods in Engineering*, 14 (1998) 1133-1141.
- [22] L. Xiao-song, Y. Wen-bo, Solution of bending of cantilever rectangular plates under uniform surface-load by the method of two-direction trigonometric series, *Applied Mathematics and Mechanics*, 6 (1985) 789-799.